Available online at www.sciencedirect.com
ScienceDirect
Journal of Computational Physics 219 (2006) 715–732
JOURNAL OF COMPUTATIONAL PHYSICS
www.elsevier.com/locate/jcp

Implementation of WENO schemes in compressible multicomponent flow problems

Eric Johnsen *, Tim Colonius

Division of Engineering and Applied Science, California Institute of Technology, Pasadena, CA 91125, United States

Received 29 July 2005; received in revised form 7 April 2006; accepted 12 April 2006

Abstract

High-order accurate shock-capturing schemes are capable of properly resolving discontinuities with correct wave speeds in single-fluid Riemann problems. However, when different fluids are present, oscillations develop at interfaces. A class of existing interface-capturing methods that suppress these oscillations is based on first- and second-order accurate reconstructions with Roe solvers. In this paper, we extend these methods to high-order accurate WENO schemes and the HLLC approximate Riemann solver. In particular, we show that a finite volume formulation where the appropriately averaged primitive variables are reconstructed leads to the oscillation-free advection of an isolated interface. Furthermore, numerical experiments show no spurious oscillations for problems where shockwaves and interfaces interact. We solve the Euler equations supplemented by a stiffened equation of state to model flows of gas and liquid components. Our method is high-order accurate, quasi-conservative, shock-capturing and interface-capturing; these properties are additionally verified by considering one-dimensional multicomponent Riemann problems and a two-dimensional shock–bubble interaction.

MSC: 76M12; 76T10

Keywords: Multicomponent flows; Interface capturing; Interface oscillations; Shock–bubble interaction; WENO; HLLC solver

1. Introduction

High-order accurate shock-capturing schemes are widely used in computational fluid dynamics to resolve compressible flow features that involve both shockwaves and complex smooth structures. In particular, the popular finite difference and finite volume essentially non-oscillatory (ENO) [17,36] and Weighted ENO (WENO) [19,27] methods perform well in such problems. They prevent oscillations near shockwaves without introducing excessive dissipation and offer very high resolution in smooth regions. This latter point is a serious drawback of first- and second-order accurate methods [38]. However, naive implementations of the aforementioned schemes in compressible multicomponent flow problems give rise to oscillations at material interfaces.

* Corresponding author. Tel.: +1 626 395 4153.
E-mail addresses: ejohnsen@caltech.edu (E. Johnsen), colonius@caltech.edu (T. Colonius).

0021-9991/$ - see front matter
doi:10.1016/j.jcp.2006.04.018

In early algorithms for computing compressible multicomponent flows, the discontinuous nature of the fluid composition is represented by the mass fraction [23], the ratio of specific heats [20], or a level-set function [30], and evolved according to an advection equation coupled to the Euler equations. The resulting system is solved using first- and second-order accurate reconstructions with a Roe solver [34]. However, spurious oscillations develop at interfaces. The cause of these oscillations is identified in [1], where a quasi-conservative method based on the mass fraction formulation is proposed for gases; subsequently, this has been extended to more general equations of state [39,35,40], and to multiphase [3] and reactive flows [6]. The difficulty resides in maintaining the pressure equilibrium across the interface despite numerical dissipation [20] and in coupling advection equations to the Euler system in a consistent fashion [1,11]. The implementation of non-oscillatory methods, such as the finite difference WENO scheme in [28], does not suppress these oscillations.

In analogy to shock-capturing, the methods described above are termed interface-capturing, as the interface is not explicitly tracked but allowed to diffuse numerically. Sharp interfaces can be achieved using interface-tracking methods, where a level set function [31] usually tracks the interface. However, such formulations often involve slight modifications to the governing equations. In [20,21], the energy equation is replaced by a pressure evolution equation near interfaces. In the Ghost Fluid Method [10] and simplified versions thereof [2,22], thermodynamically similar variables are added across interfaces to complete stencils. In [18], the internal energy is corrected based on an updated value of the ratio of specific heats. These methods do not generate spurious oscillations at interfaces and can be used with WENO schemes. However, they are not discretely conservative [2,26], making them less desirable for problems where shockwaves are involved.

Our goal is to simulate compressible multicomponent flow problems while satisfying certain important properties mentioned above. First, in order to avoid spurious oscillations near shockwaves and interfaces, we seek shock- and interface-capturing or -tracking capabilities. Also, we wish to enforce conservation in the discretized Euler equations. In addition, in order to be able to resolve complicated flow features with shockwaves, we require our method to be high-order accurate. Finally, from a practical standpoint, the scheme should also be computationally efficient and easy to implement.

In order to achieve these goals, we have extended existing quasi-conservative interface-capturing methods [1,39] by implementing a high-order accurate WENO reconstruction and the positivity-preserving HLLC solver [45,44]. The governing equations for multicomponent flows are stated in Section 2 and the bases of our numerical scheme are presented in Section 3. In Section 4, we examine the mechanism responsible for interface oscillations and describe how these are suppressed. Our method is validated using benchmark problems in Section 5. Finally, we summarize our findings and present an outlook for future studies.

2. Equations of motion

Multicomponent flows are a subset of multiphase flows where the different fluid components, characterized by their respective (constant) ratio of specific heats, are immiscible; diffusive effects, surface tension and cavitation are neglected. The Euler equations govern such multicomponent flows, written here in one dimension for simplicity:

$$\mathbf{q}_t + \mathbf{f}(\mathbf{q})_x = \mathbf{0}, \quad \mathbf{q}(x,t) = (\rho, \rho u, E)^{\mathrm{T}}, \quad \mathbf{f}(\mathbf{q}) = (\rho u, \rho u^2 + P, u(E+P))^{\mathrm{T}}, \tag{1}$$

where ρ is the density, u the velocity, P the pressure and E the total energy of the fluid. To close the system, we use the stiffened equation of state [15],

$$\Gamma P + \Pi_\infty = E - \frac{1}{2}\rho u^2, \quad \Gamma = \frac{1}{\gamma - 1}, \quad \Pi_\infty = \frac{\gamma P_\infty}{\gamma - 1}. \tag{2}$$

For perfect gases, γ is the ratio of specific heats and $P_\infty = 0$; for water, $\gamma = 5.5$ and $P_\infty = 4921.15$ bar [7]. This equation of state is thermodynamically consistent [29] and has been used extensively to model[1] multicomponent flows with shockwaves [7,39,35,2]. The interface between two fluids is represented by the discontinuity in

[1] As pointed out by a referee, whether this equation of state is thermodynamically consistent when the interface diffuses numerically is unclear. Although this issue is beyond the scope of this paper, we nevertheless remark that in the limit, $\Delta x \to 0$, the interface converges to a sharp one, leading us to expect appropriate behavior.

the properties, γ and P_∞, of the different fluid components. Since material interfaces are advected by the flow, Γ and Π_∞ obey the advection equation [1,39],

$$\boldsymbol{\phi}_t + u\boldsymbol{\phi}_x = 0, \quad \boldsymbol{\phi} = (\Gamma, \Pi_\infty)^{\mathrm{T}}. \tag{3}$$

Eqs. (1) and (3) form a quasi-conservative system [39]. The Euler equations (1) are conservative, ensuring that ρ, ρu and E are conserved, while the advection equations (3), which are non-conservative, specify the correct location of the interface, so that the relevant properties are defined. Although not fully conservative, the system conserves the required physical quantities.

We note that the advection equations (3) can be combined with the continuity equation to form conservative equations,

$$(\rho\boldsymbol{\phi})_t + (\rho u\boldsymbol{\phi})_x = 0, \tag{4}$$

where $\boldsymbol{\phi}$ could be any function of γ and P_∞. The system (1) and (4) is fully conservative. However, it is shown in Section 4.1 that this coupling will generate oscillations at interfaces using standard shock-capturing schemes, and that Γ and Π_∞ must be advected.

3. Spatial discretization

3.1. Finite volume vs. conservative finite difference approximations

We follow [37] to compare finite volume (FV) and conservative finite difference (FD) ENO and WENO approximations. We will show in Section 4 that a FV formulation must be used to suppress oscillations generated at interfaces, so we describe it in greater detail in the following sections. In the computational cell, $I_i = [x_i - \Delta x/2;\ x_i + \Delta x/2]$, Eq. (1) can be written in semi-discrete form,

$$\frac{\mathrm{d}\tilde{\mathbf{q}}_i}{\mathrm{d}t} = -\frac{\mathbf{f}_{i+1/2} - \mathbf{f}_{i-1/2}}{\Delta x}, \tag{5}$$

where $\tilde{\mathbf{q}}_i$ approximates the conserved variable, $\mathbf{q}$, at i, and $\mathbf{f}_{i+1/2}$ approximates the flux, $\mathbf{f}(\mathbf{q})$, at the cell edge, $i+1/2$. In the FV formulation, $\tilde{\mathbf{q}}_i$ is the cell average value of $\mathbf{q}$ in I_i, and is reconstructed on either side of each cell edge, thus yielding a Riemann problem with left and right states, $\mathbf{q}^{\mathrm{L}}_{i+1/2}$ and $\mathbf{q}^{\mathrm{R}}_{i+1/2}$. An approximate Riemann solver provides the correct upwind numerical flux. In the FD formulation, $\tilde{\mathbf{q}}_i$ is the point value of $\mathbf{q}$ at x_i, and positive and negative fluxes defined at the cell centers are interpolated at the cell edges. A flux-splitting scheme is used to compute the correct upwind numerical flux.

3.2. Finite volume reconstruction

In first-order FV methods, the left and right states of the Riemann problem are reconstructed from the cell averages in a piecewise constant fashion. Such methods can be extended to second-order accuracy by using limiters [25]. ENO reconstruction [17,36] is based on adaptive stencils, such that the optimal stencil is chosen. Given the cell average values of a function, the function is interpolated on either side of the cell edges. This provides high-order accuracy and essentially non-oscillatory behavior. WENO reconstruction [19,27] consists of a convex combination of all the candidate stencils, and constitutes an improvement on ENO schemes on many levels [19,38].

The reconstruction is often performed in characteristic space because of the self-similar nature of the Riemann problem for the Euler equations (1). In systems of nonlinear equations, oscillations can develop in component-wise reconstruction due to the interaction of discontinuities of different characteristic fields, regardless of the CFL constraint [17,32]. The characteristic form of the Euler equations is

$$\frac{\partial \mathbf{w}}{\partial t} + \Lambda\frac{\partial \mathbf{w}}{\partial x} = 0, \tag{6}$$

where

$$d\mathbf{w} = \left(du - \frac{dP}{\rho c}, d\rho - \frac{dP}{c^2}, du + \frac{dP}{\rho c}\right)^{\mathrm{T}}, \quad \Lambda = \mathrm{Diag}[u - c, u, u + c]. \tag{7}$$

We note that the advection equations are already in characteristic form. The variables are first locally decomposed onto the respective characteristic fields and then reconstructed; thereafter, they are projected back into physical space [37]. Although this reconstruction is more expensive computationally, each field is treated separately, thus avoiding collisions between characteristics.

Multi-dimensional ENO and WENO schemes can easily be implemented in the FD formulation dimension by dimension [37]. However, a two-dimensional FV reconstruction is computationally intensive, because two one-dimensional reconstructions are needed per grid point [37]. Since the fluxes must be averaged along the cell edges, a Gaussian quadrature rule is used in multiple dimensions [13,43].

3.3. The HLLC approximate Riemann solver

Because the Riemann problem resulting from the reconstruction is computationally expensive to solve exactly, an approximate Riemann solver is used. Examples thereof include the Roe [34] and HLL [16] solvers; the Lax–Friedrichs solver is a special case of the HLL solver [44]. Roe solvers are less dissipative, but more computationally intensive. More importantly, they do not preserve positivity [8]. This is a critical property when computing problems where low densities and pressures are achieved, which can occur in a number of compressible multicomponent flow calculations. Thus, we favor HLL solvers, in particular the HLLC solver [45], because it resolves discontinuities sharply, and isolated shockwaves and contacts exactly [5]. Given allowable left and right states, the HLLC solver preserves positivity [5]. By definition, WENO is a convex reconstruction of the candidate stencils [19]. Therefore, given that the cell average values are in an allowable physical set, the left and right states generated by WENO will be in this allowable set as well, so that the overall scheme preserves positivity.

The HLLC solver is an extension to the HLL solver, whereby the contact discontinuity is restored [45,44]. The HLLC flux can be written:

$$\mathbf{f}^{\mathrm{HLLC}} = \frac{1 + \mathrm{sign}(s^*)}{2}\left[\mathbf{f}^{\mathrm{L}} + s^-\left(\mathbf{q}^{*\mathrm{L}} - \mathbf{q}^{\mathrm{L}}\right)\right] + \frac{1 - \mathrm{sign}(s^*)}{2}\left[\mathbf{f}^{\mathrm{R}} + s^+\left(\mathbf{q}^{*\mathrm{R}} - \mathbf{q}^{\mathrm{R}}\right)\right], \tag{8}$$

where the intermediate "star" state is defined as

$$\mathbf{q}^{*k} = \chi^{*k}\begin{pmatrix} \rho^k \\ \rho^k s^* \\ E^k + (s^* - u^k)\left(\rho^k s^* + \frac{P^k}{s^k - u^k}\right) \end{pmatrix}, \quad \chi^{*k} = \frac{s^k - u^k}{s^k - s^*}, \tag{9}$$

where $k = \mathrm{L}, \mathrm{R}$. Following [8], the wave speeds are given by:

$$s^- = \min(0, s^{\mathrm{L}}), \quad s^+ = \max(0, s^{\mathrm{R}}), \tag{10}$$

where

$$s^{\mathrm{L}} = \min\left((u - c)^{\mathrm{ROE}}, u^{\mathrm{L}} - c^{\mathrm{L}}\right), \quad s^{\mathrm{R}} = \max\left((u + c)^{\mathrm{ROE}}, u^{\mathrm{R}} + c^{\mathrm{R}}\right). \tag{11}$$

The intermediate wave speed is computed according to [5],

$$s^* = \frac{P^{\mathrm{R}} - P^{\mathrm{L}} + \rho^{\mathrm{L}} u^{\mathrm{L}}(s^{\mathrm{L}} - u^{\mathrm{L}}) - \rho^{\mathrm{R}} u^{\mathrm{R}}(s^{\mathrm{R}} - u^{\mathrm{R}})}{\rho^{\mathrm{L}}(s^{\mathrm{L}} - u^{\mathrm{L}}) - \rho^{\mathrm{R}}(s^{\mathrm{R}} - u^{\mathrm{R}})}. \tag{12}$$

3.4. Adapting the HLLC solver to the advection equation

Although hyperbolic, advection equations are not conservation laws, so it is not immediately clear how to implement any approximate Riemann solver consistently with the Euler equations. The Lax–Friedrichs, Roe

and HLL solvers have previously been adapted to the advection equation [1,39,35]. In order to adapt the HLLC solver, it is tempting follow the same thought process by considering two states connected by a wave moving at speed, u_i. Eq. (3) becomes, in semi-discrete form,

$$\frac{\mathrm{d}\overline{\boldsymbol{\phi}}_i}{\mathrm{d}t} = -\frac{u_i}{\Delta x}\left[\frac{1+\mathrm{sign}(u_i)}{2}\left(\boldsymbol{\phi}^{\mathrm{L}}_{i+1/2} - \boldsymbol{\phi}^{\mathrm{L}}_{i-1/2}\right) + \frac{1-\mathrm{sign}(u_i)}{2}\left(\boldsymbol{\phi}^{\mathrm{R}}_{i+1/2} - \boldsymbol{\phi}^{\mathrm{R}}_{i-1/2}\right)\right]. \tag{13}$$

It is easy to verify that this leads to the oscillation-free advection of an isolated interface and propagation of isolated shocks. However, if the pressure varies strongly for non-constant $\boldsymbol{\phi}$, the wavespeed in the advection equation, u_i, is inconsistent with that of the contact discontinuity, $s^*_{i\pm1/2}$, in the Euler equations. To overcome this difficulty, we use the chain rule to write Eq. (3) as

$$\boldsymbol{\phi}_t + \mathbf{g}_x - \boldsymbol{\phi} u_x = 0, \quad \mathbf{g} = u\boldsymbol{\phi}. \tag{14}$$

The second term is a conservative flux, and the velocity differentiation in the third term enables us to adapt the HLLC solver. Integrating the advection equation (14) over a cell, i, we obtain

$$\left.\frac{\mathrm{d}\overline{\boldsymbol{\phi}}}{\mathrm{d}t}\right|_i = -\frac{1}{\Delta x}\left(\mathbf{g}_{i+1/2} - \mathbf{g}_{i-1/2}\right) + \frac{1}{\Delta x}\int_{x_i-1/2}^{x_i+1/2} \boldsymbol{\phi}\frac{\partial u}{\partial x}\mathrm{d}x. \tag{15}$$

This equation is exact. We make the following approximation to evaluate the integral:

$$\left.\frac{\mathrm{d}\overline{\boldsymbol{\phi}}}{\mathrm{d}t}\right|_i = -\frac{1}{\Delta x}\left(\mathbf{g}_{i+1/2} - \mathbf{g}_{i-1/2}\right) + \frac{1}{\Delta x}\overline{\boldsymbol{\phi}}_i\left(u_{i+1/2} - u_{i-1/2}\right). \tag{16}$$

Eq. (16) is exact far from interfaces, where $\boldsymbol{\phi}$ is assumed constant. At discontinuities, shock-capturing schemes can achieve no better than first-order accuracy [25]; since the integral in Eq. (15) is evaluated using a midpoint rule and the derivative using a centered scheme, it is at worst second-order accurate. Therefore, this approximation does not deteriorate the overall order of accuracy of the method. Based on the conservative form of the advection equation [44], we compute the velocity in the source term as

$$u^{\mathrm{HLLC}} = \frac{1+\mathrm{sign}(s^*)}{2}\left[u^{\mathrm{L}} + s^-(\chi^{*\mathrm{L}} - 1)\right] + \frac{1-\mathrm{sign}(s^*)}{2}\left[u^{\mathrm{R}} + s^+(\chi^{*\mathrm{R}} - 1)\right]. \tag{17}$$

4. Interface capturing

4.1. Occurrence of oscillations at isolated interfaces

Since our scheme is shock-capturing, isolated shockwaves and rarefaction waves are treated appropriately. Across isolated material interfaces, the model equations (1) and (3) preserve the pressure equilibrium [39]. Our goal is to provide a spatial discretization scheme that satisfies this condition.

To motivate our numerical method, we follow [1,2,39] and consider the problem of the advection of an isolated interface between two different gases at constant speed. The kinematic and dynamic interface conditions require u and P to be uniform in time and space; therefore the Euler equations (1) become:

$$\frac{\partial \rho}{\partial t} = -u\frac{\partial \rho}{\partial x}, \tag{18a}$$

$$\frac{\partial (\rho u)}{\partial t} = -u^2\frac{\partial \rho}{\partial x}, \tag{18b}$$

$$\frac{\partial E}{\partial t} = -u\left(\frac{u^2}{2}\frac{\partial \rho}{\partial x} + P\frac{\partial \Gamma}{\partial x}\right). \tag{18c}$$

Combining Eqs. (18a) and (18b), we obtain $\mathrm{d}u/\mathrm{d}t = 0$. Eq. (18c) and the equation of state (2) yield $\mathrm{d}P/\mathrm{d}t = 0$ if

$$\frac{\partial \Gamma}{\partial t} = -u\frac{\partial \Gamma}{\partial x}. \tag{19}$$

In FV methods, the conservative variables, $\mathbf{q} = (\rho, \rho u, E, \rho\Gamma)^{\mathrm{T}}$, are reconstructed. However, the numerical dissipation introduced in these variables, in particular in E and $\rho\Gamma$, does not maintain the pressure equilibrium

[20,35], especially when using a nonlinear reconstruction such as WENO. For the same reason, FD methods fail, because the fluxes are interpolated. In order to preserve the pressure equilibrium in the discrete equations, we emulate the behavior of the continuous equations (18) and (19) by reconstructing u and P individually. Since the elements of the interpolating stencils are identical near isolated interfaces, the equilibrium in these variables is preserved. Thus, we conclude that *the primitive variables*, $\mathbf{u} = (\rho, u, P, \Gamma)^{\mathrm{T}}$, *must be reconstructed*, rather than $\mathbf{q}$.

This has further implications for the advection equation. First, the specific function, $\Gamma(\gamma) = 1/(\gamma - 1)$, must be advected, not just any arbitrary function of γ [39]. Thus, model equations (1) and (3) must be used. Also, the advection equation must be discretized in a fashion consistent with the energy equation [1,35]. Coupling a level set equation as in [11] does not necessarily guarantee this requirement and thus might cause oscillations. It is straightforward to treat the case of Π_∞ in an analogous fashion [39].

This analysis shows that if the above conditions are not met a discontinuity in Γ causes an error in pressure at the interface, which generates oscillations that propagate with the flow. Methods where there is no explicit discontinuity in Γ (e.g., Ghost Fluid Methods [10,2]) or where Γ does not enter the equations at interfaces (e.g., Pressure Evolution methods [20,21]) are not affected by this problem.

4.2. Reconstruction of the primitive variables

At the beginning of each time step, we are given the cell averages of the conservative quantities. In order to reconstruct the primitive variables, we define local average velocity, $\bar{v}$, and pressure, $\bar{p}$,

$$\bar{v}_i \triangleq \frac{\overline{\rho u}_i}{\bar{\rho}_i}, \quad \bar{p}_i \triangleq \frac{\overline{E}_i - \bar{\rho}_i \frac{\bar{v}_i^2}{2}}{\overline{\Gamma}_i}. \tag{20}$$

The average velocity, $\bar{v}$, is analogous to the density-weighted (Favre [9]) average used in compressible turbulence models. These variables, along with $\bar{\rho}_i$ and $\overline{\Gamma}_i$, are reconstructed using WENO. This provides the left and right states for the Riemann problem at the cell edges.

To understand the impact of this methodology on the accuracy of the scheme, we define the sliding average of a function, $q(x)$, by

$$\bar{q}(x) \triangleq \frac{1}{\Delta x} \int_{x-\Delta x/2}^{x+\Delta x/2} q(\xi)\, \mathrm{d}\xi, \quad \bar{q}_i = \bar{q}(x_i), \tag{21}$$

so that in smooth regions, $\bar{q}(x) = q(x) + \mathrm{O}(\Delta x^2)$. ENO and WENO reconstructions have the following property [17,37]:

$$\overline{\tilde{q}}(x_i) = \bar{q}_i, \tag{22}$$

where $\tilde{q}(x)$ is a pointwise approximation to $q(x)$. Therefore, the reconstruction preserves the total amount of q in each cell. Eq. (21) implies that $\bar{u}(x) = u(x) + \mathrm{O}(\Delta x^2)$. Using Taylor series expansion, we observe that $\bar{v}(x) = u(x) + \mathrm{O}(\Delta x^2)$, so that $\bar{v}$ approximates $u(x)$ to the same order that $\bar{u}$ does. This justifies the definitions in Eq. (20), which are the building blocks of the reconstruction. From Eq. (22), given the reconstructed density, $\tilde{\rho}(x)$, and momentum, $\widetilde{\rho u}(x)$, the reconstructed velocity, $\tilde{v}(x)$, satisfies

$$\overline{\tilde{\rho}}(x)\overline{\tilde{v}}(x) = \overline{\widetilde{\rho u}}(x). \tag{23}$$

In other words, $\tilde{v}(x)$ is a high-order accurate approximation to the velocity, which preserves the total momentum in each cell. Therefore, $\rho u_{i+1/2} = \rho_{i+1/2} v_{i+1/2}$ to high-order accuracy. Similarly, $\tilde{p}(x)$ is a high-order accurate approximation to the pressure, which preserves the total energy in each cell. The convergence analysis presented in Section 5.1 indicates that the proper convergence rate is achieved. Characteristic reconstruction can easily be implemented, as the characteristic variables are naturally expressed in terms of primitive variables. Finally, we remark that the Euler equations (1) are still written in flux difference form [25],

$$\mathbf{f}_{i+1/2} = \mathbf{f}_{(i+1)-1/2}. \tag{24}$$

Eqs. (23) and (24) show that the numerical scheme is discretely conservative [25] for the Euler equations.

4.3. Oscillation-free advection of an isolated interface

We show that our scheme maintains pressure equilibrium for the problem of the advection of an isolated interface between two gases at constant speed, u. Without loss of generality, we consider the case $|s^k| > u > 0$, so that $\mathbf{q}^{*\mathrm{L}} = \mathbf{q}^{\mathrm{L}}$ and $u^{*\mathrm{L}} = u^{\mathrm{L}} = u$. From the interface conditions, the velocity, u, and the pressure, P, are uniform. Then, using the HLLC solver (8) and (17) and the reconstruction of the primitive variables described above, the Euler and advection equations (1) and (3) can be marched forward by a time step:

$$\bar{\rho}_i^{n+1} = \bar{\rho}^n - \frac{\Delta t}{\Delta x} u\left(\rho_{i+1/2}^{\mathrm{L}} - \rho_{i-1/2}^{\mathrm{L}}\right), \tag{25a}$$

$$\overline{\rho u}_i^{n+1} = \overline{\rho u}_i^n - \frac{\Delta t}{\Delta x} u^2\left(\rho_{i+1/2}^{\mathrm{L}} - \rho_{i-1/2}^{\mathrm{L}}\right), \tag{25b}$$

$$\overline{E}_i^{n+1} = \overline{E}_i^n - \frac{\Delta t}{\Delta x} u\left[\frac{u^2}{2}\left(\rho_{i+1/2}^{\mathrm{L}} - \rho_{i-1/2}^{\mathrm{L}}\right) + P\left(\Gamma_{i+1/2}^{\mathrm{L}} - \Gamma_{i-1/2}^{\mathrm{L}}\right)\right], \tag{25c}$$

$$\overline{\Gamma}_i^{n+1} = \overline{\Gamma}_i^n - \frac{\Delta t}{\Delta x} u\left(\Gamma_{i+1/2}^{\mathrm{L}} - \Gamma_{i-1/2}^{\mathrm{L}}\right). \tag{25d}$$

Since u is constant, $\overline{\rho u}_i^n = \bar{\rho}_i^n u$. The equation of state (2) and Eq. (25) can be combined to yield the velocity and pressure at the next time step:

$$u_i^{n+1} \triangleq \frac{\overline{\rho u}_i^{n+1}}{\bar{\rho}_i^{n+1}} = u, \tag{26a}$$

$$P_i^{n+1} \triangleq \frac{\overline{E}_i^{n+1} - \frac{\left(\overline{\rho u}_i^{n+1}\right)^2}{2\bar{\rho}_i^{n+1}}}{\overline{\Gamma}_i^{n+1}} = P. \tag{26b}$$

Therefore, our scheme maintains equilibrium in velocity and pressure for the advection of an isolated interface. This can be generalized to fluids with $P_\infty \neq 0$ and to multiple dimensions. However, we note that this cannot readily be extended to problems where interfaces interact with shockwaves; nevertheless, we demonstrate in the difficult test cases of Section 5 that no oscillations are observed.

4.4. Algorithm

In light of the preceding sections, we propose the following algorithm to compute compressible multicomponent flows, based on the model equations (1) and (3). Given the cell averages, $\bar{\mathbf{q}}_i$ and $\overline{\boldsymbol{\phi}}_i$, at some time step

(1) Build the average primitive variables, $\overline{\mathbf{u}}_i$.
(2) Using WENO, reconstruct the primitive variables, $\mathbf{u}_{i+1/2}^{\mathrm{L}}$ and $\mathbf{u}_{i+1/2}^{\mathrm{R}}$.
(3) Build the conservative variables, $\mathbf{q}_{i+1/2}^{\mathrm{L}}$ and $\mathbf{q}_{i+1/2}^{\mathrm{R}}$, and the fluxes $\mathbf{f}_{i+1/2}^{\mathrm{L}}$ and $\mathbf{f}_{i+1/2}^{\mathrm{R}}$.
(4) Use the HLLC solver to compute the numerical flux, $\mathbf{f}_{i+1/2}$.
(5) Use the adaptation to the HLLC solver to compute the right-hand side of the advection equations.
(6) March $\bar{\mathbf{q}}_i$ and $\overline{\boldsymbol{\phi}}_i$ forward in time.

This procedure requires approximately the same number of operations as a normal WENO code, and is no more difficult to implement. The reconstruction can be applied to the local characteristic fields [37]; however the transformation matrices are those relating to the primitive variables. This is done by multiplying $\overline{\mathbf{u}}_i$ by the left Roe matrix after step one, and $\mathbf{u}_{i+1/2}^{\mathrm{L}}$ and $\mathbf{u}_{i+1/2}^{\mathrm{R}}$ by the right Roe matrix after step two.

This algorithm can be extended to multiple dimensions. After the WENO reconstruction, $\mathbf{u}_{i+1/2,j}^{\mathrm{L}}$ and $\mathbf{u}_{i+1/2,j}^{\mathrm{R}}$ are reconstructed in the transverse direction, thus yielding the values at $j \pm 1/2\sqrt{3}$ required by the Gaussian quadrature for the numerical fluxes [13,43].

5. Results

In the following test cases, we compare the present method with our implementation of FD and FV WENO schemes. The main differences lie in the model equations used and the variables that are interpolated or reconstructed using WENO, as shown in Table 1. The FD and fully conservative schemes are implemented using existing methods [37] and are expected to behave in a similar fashion, since the model equations are identical. The quasi-conservative FV scheme is implemented following [35] and is expected to generated smaller oscillations than the former schemes. The present scheme follows Algorithm 4.4 and is not expected to generate oscillations. The time-marching is handled by a third-order TVD Runge–Kutta scheme [12,36], unless otherwise specified. We denote by WENOr a WENO scheme of order r. The grid and time stepping are uniform, with $\Delta t/\Delta x = 0.2$ for simplicity.

5.1. Convergence analysis

In order to assess the convergence of the present method with respect to that of the quasi-conservative FV scheme in Table 1, we consider an acoustics problem in a single gas component. We perturb the primitive variables about a base state:

$$\rho(x,t) = \rho_0 + \epsilon\rho'(x,t), \quad u(x,t) = \epsilon u'(x,t), \quad P(x,t) = P_0 + \epsilon P'(x,t), \tag{27}$$

where ϵ is small. Using conservation of mass and momentum, and the equation of state,

$$\left.\frac{\partial P}{\partial \rho}\right|_s = c^2, \tag{28}$$

where c is the speed of sound, it can be shown that ρ', u' and P' satisfy the second-order wave equation, with wave speed c_0, to first order in ϵ. We start with an initial perturbation, $f(x) = \sin^8(\pi x)$, such that the initial conditions are

$$\rho(x,0) = 1 + \epsilon f(x), \quad u(x,0) = 0, \quad P(x,0) = \frac{1}{\gamma} + \epsilon f(x). \tag{29}$$

As ϵ increases, the wave steepens and ultimately breaks, so that a shockwave forms. When $\epsilon \approx 0.4$, the wave breaks within a period.

Figs. 1 and 2 compare the L_1 and L_∞ errors in density between the present scheme and the quasi-conservative FV scheme for $\epsilon = 10^{-4}$ and $\epsilon = 0.1$, respectively, after one period. To evaluate the error, we take the reference to be the computed solution with a much larger number of points ($N_{\text{exact}} = 1280$) than those we are studying ($N = 10, 20, 40, 80, 160$). WENO3 and WENO5 are implemented without characteristic reconstruction, along with the HLLC solver, though there is not much difference if characteristic reconstruction or different solvers are used [37]. The time-marching is handled using fifth-order Runge–Kutta.

The agreement between the two methods is excellent for $\epsilon = 10^{-4}$. We note a slight departure from the -5 slope near $N = 160$, as the "exact" solution is approached. The solution is still smooth for $\epsilon = 0.1$, although the wave starts to steepen, making this case more difficult to compute. As should be anticipated, the convergence rate departs from the expected slope, especially in the L_∞ plot. The present method performs slightly better than the quasi-conservative FV scheme when using WENO3, but slightly worse when using WENO5.

Table 1
Comparison between the different FD and FV WENO schemes, listing the model equations and variables that are interpolated/reconstructed using WENO

Scheme	Model	WENO variables
FD	(1) and (4)	$(\rho u, \rho u^2 + P, (E+P)u, \rho u\Gamma)^{\mathrm{T}}$
Fully conservative FV	(1) and (4)	$(\rho, \rho u, E, \rho\Gamma)^{\mathrm{T}}$
Quasi-conservative FV	(1) and (3)	$(\rho, \rho u, E, \Gamma)^{\mathrm{T}}$
Present	(1) and (3)	$(\rho, u, P, \Gamma)^{\mathrm{T}}$

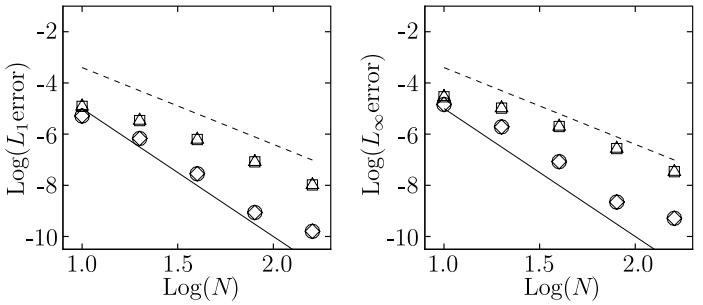

Fig. 1. L_1 and L_∞ errors in density for $\epsilon = 10^{-4}$ using WENO3 (△: quasi-conservative FV; □: present scheme) and WENO5 (◇: quasi-conservative FV; ○: present scheme); dashed and solid lines have slopes −3 and −5, respectively.

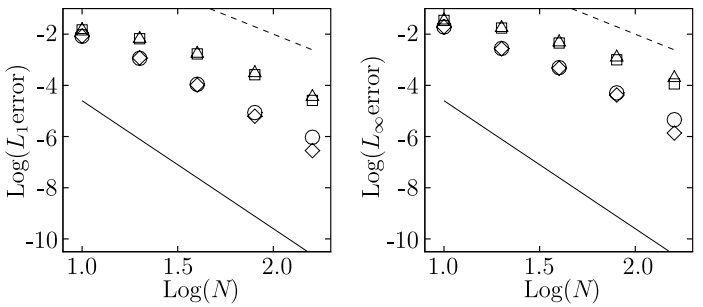

Fig. 2. L_1 and L_∞ errors in density for $\epsilon = 0.1$ using WENO3 (△: quasi-conservative FV; □: present scheme) and WENO5 (◇: quasi-conservative FV; ○: present scheme); dashed and solid lines have slopes −3 and −5, respectively.

These discrepancies indicate different sensitivity to the steepening of the waves. However, this feature is not very relevant in practical multi-dimensional computations, because the discrepancy is small and the resolution is rarely better than the highest shown here.

5.2. Isolated interface problem

We illustrate the occurrence of oscillations for a simple test case, namely the advection of a gas-gas interface, with initial states,

$$\begin{aligned}(\rho, u, P, \gamma)_{\mathrm{L}}^{\mathrm{T}} &= (1, 0.5, 1/1.4, 1.4)^{\mathrm{T}},\\ (\rho, u, P, \gamma)_{\mathrm{R}}^{\mathrm{T}} &= (10, 0.5, 1/1.4, 1.6)^{\mathrm{T}}.\end{aligned} \tag{30}$$

The domain is periodic with 100 points and WENO5 is used, without characteristic reconstruction. The Lax–Friedrichs solver and the corresponding flux-splitting [37] are implemented in an attempt to compare the schemes in Table 1. Fig. 3 shows density, velocity, pressure and γ profiles after the interface has moved the length of the domain, for the FD, fully conservative and quasi-conservative FV cases.

Oscillations develop at the interface at the first time step and propagate thereafter, even though the difference in γ is small. The FD and fully conservative schemes behave in a similar fashion and generate larger oscillations than the quasi-conservative FV scheme, as expected. Although not shown here, the magnitude of the oscillations decreases as the mesh is refined [2]. Nevertheless, the interface is advected at approximately the correct speed, despite the small errors in velocity due to the oscillations. On the other hand, no oscillations other than round-off are observed when using the present scheme, as seen in Fig. 4, where the base velocity and pressure have been subtracted. In addition, the interface propagates at the correct speed. Fig. 5 plots the residual total mass, momentum and energy for all four schemes, after subtraction of the base values. All schemes show discrete conservation to round-off error.

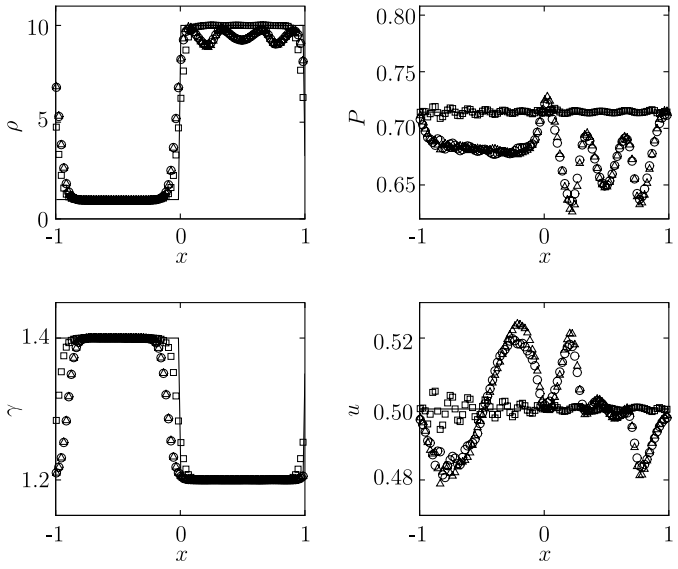

Fig. 3. Advection of a material interface (△: FD; ○: fully conservative FV; □: quasi-conservative FV); the solid line is the exact solution.

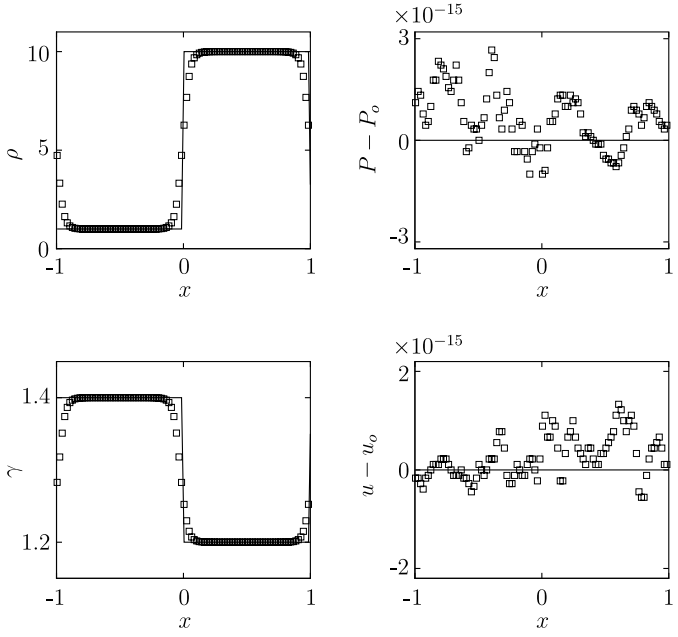

Fig. 4. Advection of a material interface using the present scheme; the solid line is the exact solution (base u and P have been subtracted).

5.3. Shock-tube problems

Although not shown here, the Sod [41] and Lax [24] problems were computed using the present scheme and produced good agreement with the analytical solution. A more difficult shock-tube problem is the following gas–liquid Riemann problem used to model underwater explosions [7,39]:

$$\begin{aligned}(\rho,u,P,\gamma,P_\infty)_{\mathrm{L}}^{\mathrm{T}} &= (1.241,0,2.753,1.4,0)^{\mathrm{T}},\\ (\rho,u,P,\gamma,P_\infty)_{\mathrm{R}}^{\mathrm{T}} &= (0.991,0,3.059\times 10^{-4},5.5,1.505)^{\mathrm{T}}.\end{aligned} \tag{31}$$

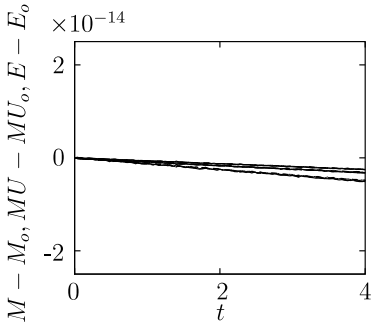

Fig. 5. Residual total mass (bottom set), momentum (top set) and energy (middle set) for the advection of a material interface, after subtraction of the base values (dotted: FD; dashed: fully conservative FV; long-dash: quasi-conservative FV; solid: present scheme).

In this problem, the gas is highly compressed, as illustrated by the large pressure and small density ratios. The domain has 100 points and WENO5 with characteristic reconstruction is used, along with the HLLC solver. Fig. 6 shows density, velocity, pressure and γ profiles at time, 0.1. We do not include P_∞ because its plot is similar to that of γ. Fig. 7 shows the residual total mass, momentum and energy, after subtraction of the base values.

The computed solution agrees well with the exact solution and compares favorably to previous findings [7,39]. The wave speeds are correct and there are no oscillations at the interface. Mass, momentum and energy are conserved to round-off error.

We now consider a multicomponent Sod problem with much larger pressure and density ratios [46]:

$$\begin{aligned}(\rho, u, P, \gamma)_{\mathrm{L}}^{\mathrm{T}} &= (10, 0, 10, 1.4)^{\mathrm{T}},\\ (\rho, u, P, \gamma)_{\mathrm{R}}^{\mathrm{T}} &= (0.125, 0, 0.1, 1.2)^{\mathrm{T}}.\end{aligned} \tag{32}$$

Fig. 8 shows density, velocity, pressure and γ profiles at time, 1.6, and Fig. 9 depicts the residual total mass, momentum and energy, after subtraction of the base values.

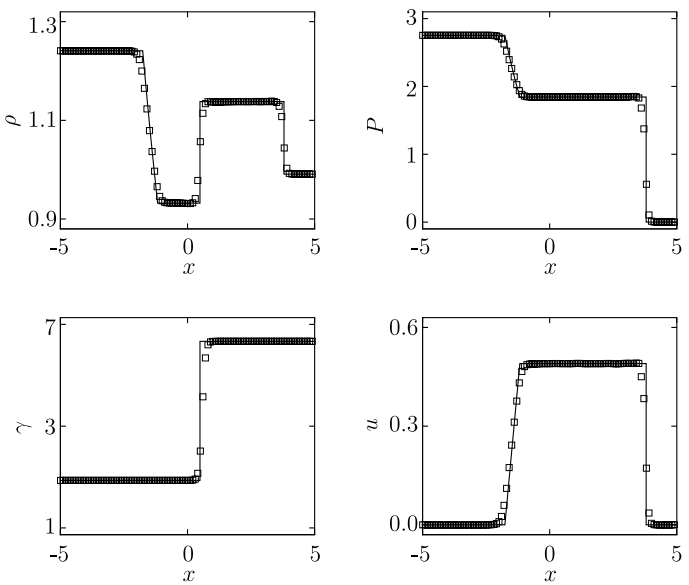

Fig. 6. Gas–liquid shock-tube problem using the present scheme at time, 0.1; the solid line is the exact solution.

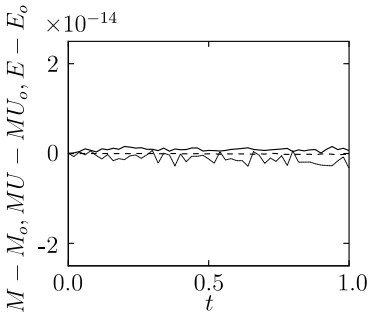

Fig. 7. Residual total mass (solid), momentum (dashed) and energy (dotted) for gas–liquid shock-tube problem using the present scheme, after subtraction of the base values.

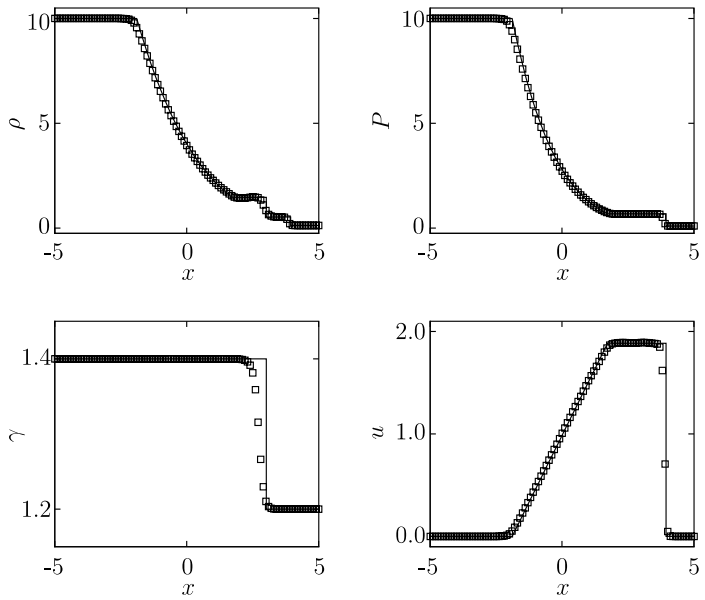

Fig. 8. Modified Sod problem using the present scheme at time, 1.6; the solid line is the exact solution.

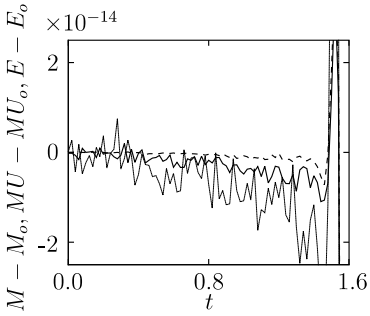

Fig. 9. Residual total mass (solid), momentum (dashed) and energy (dotted) for the modified Sod problem using the present scheme, after subtraction of the base values.

Again, the computed solution agrees very well with the exact solution. Mass, momentum and energy are conserved to round-off error; the divergence of these values at large times illustrates that the shockwave is close to the boundary. We note that in the γ plot there is more dissipation towards the left side of the interface,

because of the original density ratio; although not shown here, as N is increased, the computed solution converges to the exact solution.

5.4. Shock–bubble interaction

The previous examples show that the present method converges at the proper rate, and that the correct waves speeds are obtained in one-dimensional problems; we expect this behavior to hold in two dimensions as well. It is verified in [43] that the two dimensional FV WENO schemes converge at the proper rate. The extension of Section 4.2 to two dimensions is trivial, as the Euler equations are in flux-difference form, and the reconstruction is conservative; therefore, for two-dimensional problems similar to the previous one-dimensional problems, conservation is satisfied.

An example of two-dimensional compressible multicomponent flow is the interaction between a shockwave and a cylindrical bubble. This problem has been studied experimentally in [14], where a Mach 1.22 shockwave in air impacts upon a helium cylinder ($\rho_{He} = 0.138$, $\gamma_{He} = 1.67$). The bubble has a 50 mm diameter and the width of the shock-tube is 89 mm. Several numerical studies have been undertaken, in which a non-conservative scheme with adaptive mesh refinement [33] and a FD-WENO5 scheme [28] were used.

5.4.1. One-dimensional problem

We first consider the corresponding one-dimensional problem, to show convergence and understand the early wave interactions. WENO5 with characteristic reconstruction is used, along with the HLLC solver; non-reflecting boundary conditions [42] are implemented. Figs. 10 and 11 show density, velocity, pressure and γ profiles shortly before the left-moving transmitted shockwave leaves the domain, for the present and quasi-conservative FV schemes, respectively. Results with 100 and 400 points are presented, in order to show convergence.

The density plots depict the interface and certain waves quite well. However, a better understanding of the wave interactions is achieved by considering the pressure and velocity plots. Initially, the incident shockwave hits the bubble from the left. Upon impact, a shockwave is transmitted into the bubble, whereas an expansion wave is reflected. The shockwave inside the bubble propagates to the other interface and, upon impact, generates a transmitted shockwave and a reflected shockwave. This phenomenon continues as the reflected shockwave trapped in the bubble impacts either interface. In Figs. 10 and 11, the left-most wave is the first transmitted shockwave; the next wave is the second transmitted shockwave, after two reflections off the inter-

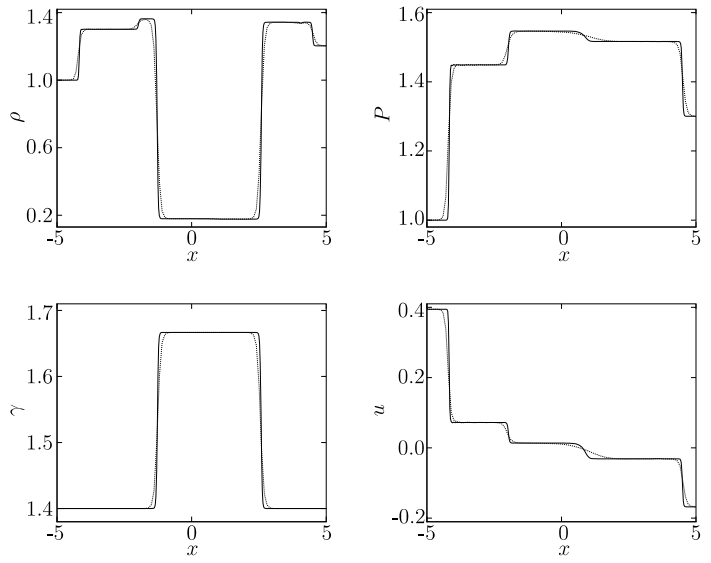

Fig. 10. One-dimensional shock–bubble interaction, using the present scheme (dotted: $N = 100$; solid: $N = 400$).

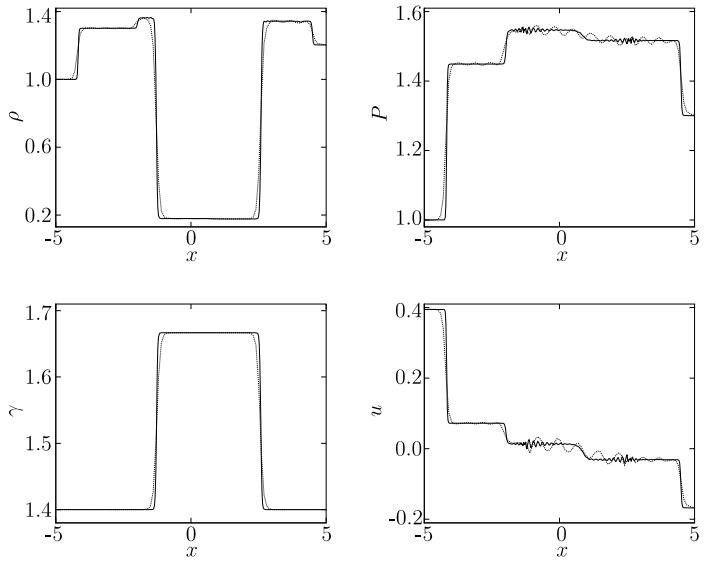

Fig. 11. One-dimensional shock–bubble interaction, using the quasi-conservative FV scheme (dotted: $N = 100$; solid: $N = 400$).

face; the next wave is the internally reflected shockwave after three reflections; the right-most wave is the first transmitted shockwave, after one reflection upon the far interface. The two left-most waves are propagating to the left and the two right-most to the right.

The quasi-conservative FV scheme clearly exhibits unacceptable oscillations, especially in the pressure and velocity. On the other hand, such oscillations do not occur when using the present scheme. Both schemes converge; the amplitude of the oscillations present in the former scheme decreases as the mesh is refined [2].

5.4.2. Two-dimensional problem

For the two-dimensional problem, an 800×400 grid is used, with reflecting boundary conditions on the top and along the centerline. The initial conditions are specified from a FV discretization. For a given radius, the appropriate properties are assigned inside and outside the bubble. Any cell that is crossed by the interface is given properties weighted by the fraction of both fluids. The initial shockwave is a straight discontinuity, with no smoothing.

We present idealized Schlieren images [33,28], which allow the visualization of the general wave structure, and density lines, which show the details of the flow, in Fig. 12 for the present scheme. Frame A is taken shortly after the shockwave has impacted the bubble, frame B shortly before the first transmitted shockwave has left the domain, frame C shortly before the first reflection from the top wall leaves the domain and frame D at a later time. The pressure along the horizontal centerline and the vertical line at the middle of the domain are plotted in Fig. 13 at times corresponding to frames A and B, respectively.

The results are in good qualitative agreement with [14,33,28]. The first wave interactions (frame A) and the subsequent reflections off the wall and interface (frame B) are well captured. The Kelvin–Helmholtz instability that develops along the interface and the jet formation (frames C and D) are consistent with prior findings. The high-order accurate scheme allows the complex patterns due to the wave interactions to be well resolved; no spurious oscillations are observed at interfaces or shockwaves. We note in passing that the start-up error generated by the initial discontinuity [4] is advected by the flow, but has no dynamical effect. This could have been avoided by starting the shockwave farther from the bubble [33], or by breaking a wave to form a shockwave.

On the other hand, Fig. 14 shows that, when the quasi-conservative FV scheme is used, oscillations are generated at the interface in the form of spurious waves (frame A), as in the one-dimensional problem. Their main dynamical effect is to perturb the interface; this triggers the Kelvin–Helmholtz instability earlier than expected (frames B and C), as might be the case with the scheme of [28], which does not strictly suppress oscillations.

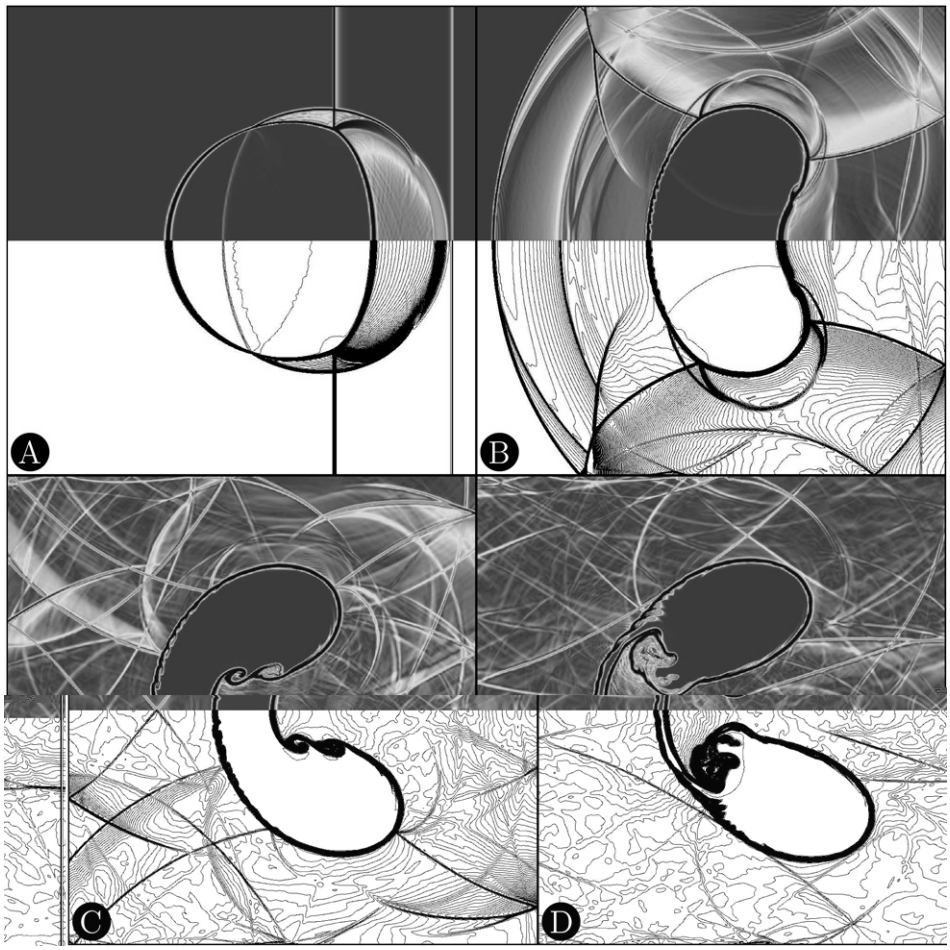

Fig. 12. Idealized Schlieren images and density lines of an interaction between a helium bubble and a Mach 1.22 shockwave in air, using the present scheme.

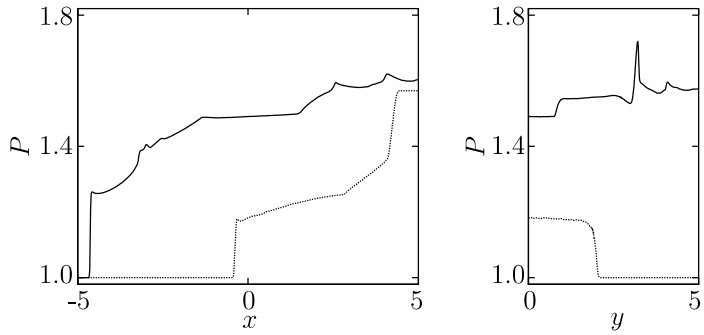

Fig. 13. Pressure along the horizontal symmetry centerline ($y = 0$) on the left and the vertical centerline ($x = 0$) on the right corresponding to frames A (dotted) and B (solid), using the present scheme.

The interface becomes more smeared, which causes a decrease in the strength of the wave fronts that pass through it. These undesirable features do not occur when using the present method. We briefly note that the slight jaggedness of the two thin density lines inside the bubble in frame A for both cases is due to the initial irregular contour of the bubble on a Cartesian grid.

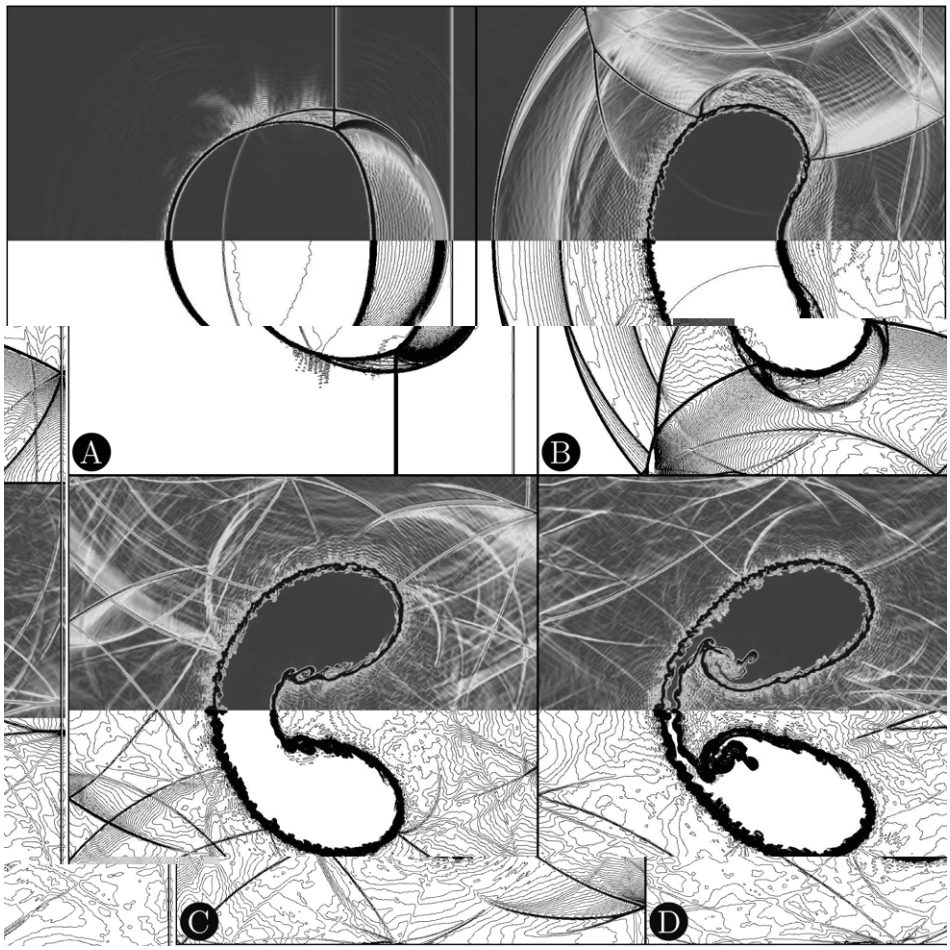

Fig. 14. Idealized Schlieren images and density lines of an interaction between a helium bubble and a Mach 1.22 shockwave in air, using the quasi-conservative FV scheme.

6. Conclusions

We have presented a high-order accurate quasi-conservative scheme, which is both shock- and interface-capturing, for computing compressible multicomponent flows. Thus, no spurious oscillations are generated at isolated shockwaves or interfaces, and smooth regions are highly resolved. Discrete conservation is enforced in the Euler equations and the advection equations are treated in a consistent fashion.

The key idea behind our method is to use a finite volume WENO formulation where the appropriately averaged primitive variables are reconstructed; the conservative reconstruction and flux-difference form in the Euler equations ensure discrete conservation. We use the positivity-preserving HLLC solver, and adapt it to the advection equations, so that it is consistent with the Euler equations; thus correct wavespeeds are obtained. Numerical experiments in one dimension verify that no conservation errors occur and that the convergence rate is correct; this can be generalized to multiple dimensions. The method is no more difficult to implement than a standard finite volume WENO scheme, nor is it more expensive computationally.

Simulating multicomponent flows to high-order accuracy, while enforcing conservation, is the first step to studying more complex systems, such as multiphase flow phenomena, where the physics must to be represented in greater detail. Surface tension, change of phase and diffusive effects, which are of considerable importance in various bubble dynamics and cavitation processes, can then be incorporated.

Acknowledgements

The authors wish to thank Randall LeVeque and Ralf Deiterding for helpful conversations. This work was supported by NIH Grant PO1 DK043881.

References

[1] R. Abgrall, How to prevent pressure oscillations in multicomponent flow calculations: a quasi conservative approach, J. Comput. Phys. 125 (1996) 150–160.
[2] R. Abgrall, S. Karni, Computations of compressible multifluids, J. Comput. Phys. 169 (2001) 594–623.
[3] R. Abgrall, R. Saurel, Discrete equations for physical and numerical compressible multiphase mixtures, J. Comput. Phys. 186 (2003) 361–396.
[4] M. Arora, P.L. Roe, On postshock oscillations due to shock capturing schemes in unsteady flows, J. Comput. Phys. 130 (1997) 25–40.
[5] P. Batten, N. Clarke, C. Lambert, D.M. Causon, On the choice of wavespeeds for the HLLC Riemann solver, SIAM J. Sci. Comput. 18 (1997) 1553–1570.
[6] G. Billet, R. Abgrall, An adaptive shock-capturing algorithm for solving unsteady reactive flows, Comput. Fluids 32 (2003) 1473–1495.
[7] J.P. Cocchi, R. Saurel, J.C. Loraud, Treatment of interface problems with Godunov-type schemes, Shock Waves 5 (1996) 347–357.
[8] B. Einfeldt, C.D. Munz, P.L. Roe, B. Sjögreen, On Godunov-type methods near low densities, J. Comput. Phys. 92 (1991) 273–295.
[9] A. Favre, Equations des gaz turbulents compressibles, J. Mec. 4 (1965) 391–421.
[10] R.P. Fedkiw, T. Aslam, B. Merriman, S. Osher, A non-oscillatory Eulerian approach to interfaces in multimaterial flows (the Ghost Fluid Method), J. Comput. Phys. 152 (1999) 457–492.
[11] R.P. Fedkiw, B. Merriman, S. Osher, Simplified discretization of systems of hyperbolic conservation laws containing advection equations, J. Comput. Phys. 157 (2000) 302–326.
[12] S. Gottlieb, C.W. Shu, Total variation diminishing Runge–Kutta schemes, Math. Comput. 67 (1998) 73–85.
[13] F. Grasso, S. Pirozzoli, Shock wave-thermal inhomogeneity interactions: analysis and numerical simulations of sound generation, Phys. Fluids 12 (2000) 205–219.
[14] J.F. Haas, B. Sturtevant, Interaction of weak shock waves with cylindrical and spherical gas inhomogeneities, J. Fluid Mech. 181 (1987) 41–76.
[15] F. Harlow, A. Amsden, Fluid Dynamics, Monograph LA-4700, Los Alamos National Laboratory, Los Alamos, NM, 1971.
[16] A. Harten, P.D. Lax, B. van Leer, On upstream differencing and Godunov-type schemes for hyperbolic conservation laws, SIAM Rev. 25 (1983) 35–61.
[17] A. Harten, B. Engquist, S. Osher, S.R. Chakravarthy, Uniformly high order accurate essentially non-oscillatory schemes III, J. Comput. Phys. 71 (1987) 231–303.
[18] P. Jenny, B. Mueller, H. Thomann, Correction of conservative Euler solvers for gas mixtures, J. Comput. Phys. 132 (1996) 91–107.
[19] G.S. Jiang, C.W. Shu, Efficient implementation of WENO schemes, J. Comput. Phys. 126 (1996) 202–228.
[20] S. Karni, Multicomponent flow calculations by a consistent primitive algorithm, J. Comput. Phys. 112 (1994) 31–43.
[21] S. Karni, Hybrid multifluid algorithms, SIAM J. Sci. Comput. 17 (1996) 1019–1039.
[22] B. Koren, M.R. Lewis, E.H. van Brummelen, B. van Leer, Riemann-problem and level-set approaches for homentropic two-fluid flow computations, J. Comput. Phys. 181 (2002) 654–674.
[23] B. Larrouturou, L. Fezoui, On the equations of multi-component perfect or real gas inviscid flow, Lecture Notes in Mathematics, vol. 1402, Springer, Heidelberg, 1989, p. 69.
[24] P. Lax, Weak solutions of nonlinear hyperbolic equations and their numerical computation, Commun. Pure Appl. Math. 7 (1954) 159–193.
[25] R.J. LeVeque, Finite Volume Methods for Hyperbolic Problems, Cambridge University Press, New York, 2002.
[26] T.G. Liu, B.C. Khoo, K.S. Yeo, Ghost fluid method for strong shock impacting on material interface, J. Comput. Phys. 190 (2003) 651–681.
[27] X.D. Liu, S. Osher, T. Chan, Weighted essentially non-oscillatory schemes, J. Comput. Phys. 115 (1994) 200–212.
[28] A. Marquina, P. Mulet, A flux-split algorithm applied to conservative models for multicomponent compressible flows, J. Comput. Phys. 185 (2003) 120–138.
[29] R. Menikoff, B.J. Plohr, The Riemann problem for fluid flow of real materials, Rev. Mod. Phys. 61 (1989) 75–130.
[30] W. Mulder, S. Osher, J.A. Sethian, Computing interface motion in compressible gas dynamics, J. Comput. Phys. 100 (1992) 209–228.
[31] S. Osher, J.A. Sethian, Fronts propagating with curvature-dependent speed: algorithms based on Hamilton–Jacobi formulations, J. Comput. Phys. 79 (1988) 12–49.
[32] J. Qiu, C.W. Shu, On the construction, comparison, and local characteristic decomposition for high-order central WENO schemes, J. Comput. Phys. 183 (2002) 187–209.
[33] J.J. Quirk, S. Karni, On the dynamics of a shock–bubble interaction, J. Fluid Mech. 318 (1996) 129–163.
[34] P.L. Roe, Approximate Riemann solvers, parameter vectors, and difference schemes, J. Comput. Phys. 43 (1981) 357–372.
[35] R. Saurel, R. Abgrall, A simple method for compressible multifluid flows, SIAM J. Sci. Comput. 21 (1999) 1115–1145.
[36] C.W. Shu, S. Osher, Efficient implementation of essentially non-oscillatory shock-capturing schemes, J. Comput. Phys. 77 (1988) 439–471.

[37] C.W. Shu, High order ENO and WENO schemes for computational fluid dynamicsHigh-Order Methods for Computational Physics, vol. 9, Springer, Heidelberg, 1999, p. 439.
[38] C.W. Shu, High-order finite difference and finite volume WENO schemes and discontinuous Galerkin methods for CFD, Int. J. Comput. Fluid Dyn. 17 (2003) 107–118.
[39] K.M. Shyue, An efficient shock-capturing algorithm for compressible multicomponent problems, J. Comput. Phys. 142 (1998) 208–242.
[40] K.M. Shyue, A fluid-mixture type algorithm for compressible multicomponent flow with Mie-Grüneisen equation of state, J. Comput. Phys. 171 (2001) 678–707.
[41] G.A. Sod, A survey of several finite difference methods for systems of nonlinear hyperbolic conservation laws, J. Comput. Phys. 27 (1978) 1–31.
[42] K.W. Thompson, Time dependent boundary conditions for hyperbolic systems, J. Comput. Phys. 68 (1987) 1–24.
[43] V.A. Titarev, E.F. Toro, Finite-volume WENO schemes for three-dimensional conservation laws, J. Comput. Phys. 201 (2004) 238–260.
[44] E.F. Toro, Riemann Solvers and Numerical Methods for Fluid Dynamics, Springer, Heidelberg, 1999.
[45] E.F. Toro, M. Spruce, W. Speares, Restoration of the contact surface in the HLL-Riemann solver, Shock Waves 4 (1994) 25–34.
[46] J. Wackers, B. Koren, A fully conservative model for compressible two-fluid flow, Int. J. Numer. Meth. Fluids 47 (2005) 1337–1343.